

RESEARCH

Inhibition of GATA2 in prostate cancer by a clinically available small molecule

Salma Kaochar^{1,2,3}, Aleksandra Rusin³, Christopher Foley^{1,3}, Kimal Rajapakshe^{2,3}, Matthew Robertson^{2,3}, Darlene Skapura¹, Cammy Mason¹, Karen Berman De Ruiz¹, Alexey Mikhailovich Tyryshkin¹, Jenny Deng¹, Jin Na Shin¹, Warren Fiskus¹, Jianrong Dong^{2,3}, Shixia Huang^{2,3,4}, Nora M Navone⁵, Christel M Davis⁶, Erik A Ehli⁶, Cristian Coarfa^{2,3} and Nicholas Mitsiades^{1,2,3}

¹Department of Medicine, Baylor College of Medicine, Houston, Texas, USA

²Dan L. Duncan Comprehensive Cancer Center, Houston, Texas, USA

³Department of Molecular and Cellular Biology, Baylor College of Medicine, Houston, Texas, USA

⁴Department of Education, Innovation, and Technology, Baylor College of Medicine, Houston, Texas, USA

⁵Division of Cancer Medicine, Department of Genitourinary Medical Oncology, The University of Texas Anderson Cancer Center, Houston, Texas, USA

⁶Avera Institute for Human Genetics, Sioux Falls, South Dakota, USA

Correspondence should be addressed to S Kaochar or N Mitsiades: salma.kaochar@bcm.edu or mitsiade@bcm.edu

Abstract

Castration-resistant prostate cancer (CRPC) remains highly lethal and in need of novel, actionable therapeutic targets. The pioneer factor GATA2 is a significant prostate cancer (PC) driver and is linked to poor prognosis. GATA2 directly promotes androgen receptor (AR) gene expression (both full-length and splice-variant) and facilitates AR binding to chromatin, recruitment of coregulators, and target gene transcription. Unfortunately, there is no clinically applicable GATA2 inhibitor available at the moment. Using a bioinformatics algorithm, we screened *in silico* 2650 clinically relevant drugs for a potential GATA2 inhibitor. Validation studies used cytotoxicity and proliferation assays, global gene expression analysis, RT-qPCR, reporter assay, reverse phase protein array analysis (RPPA), and immunoblotting. We examined target engagement via cellular thermal shift assay (CETSA), ChIP-qPCR, and GATA2 DNA-binding assay. We identified the vasodilator *dilazep* as a potential GATA2 inhibitor and confirmed on-target activity via CETSA. Dilazep exerted anticancer activity across a broad panel of GATA2-dependent PC cell lines *in vitro* and in a PDX model *in vivo*. Dilazep inhibited GATA2 recruitment to chromatin and suppressed the cell-cycle program, transcriptional programs driven by GATA2, AR, and c-MYC, and the expression of several oncogenic drivers, including AR, c-MYC, FOXM1, CENPF, EZH2, UBE2C, and RRM2, as well as of several mediators of metastasis, DNA damage repair, and stemness. In conclusion, we provide, via an extensive compendium of methodologies, proof-of-principle that a small molecule can inhibit GATA2 function and suppress its downstream AR, c-MYC, and other PC-driving effectors. We propose GATA2 as a therapeutic target in CRPC.

Key Words

- ▶ prostate cancer
- ▶ castration-resistance
- ▶ GATA2
- ▶ Dilazep
- ▶ c-MYC

Endocrine-Related Cancer
(2021) 29, 15–31

Introduction

In 2021, prostate cancer is predicted to cause the death of 34,130 US men, making it the second leading cause of cancer death in American men, after lung cancer (Siegel *et al.* 2021). Importantly, this represents a 30.6% increase in mortality compared to 2016, highlighting the unmet need for effective therapies. Progression of metastatic PC after first-line endocrine therapy is inevitable and the resulting castration-resistant PC (CRPC) is incurable and highly lethal. Second-line therapies provide small extensions of survival, while immunotherapy has not delivered in this area the significant benefits it afforded to patients with other malignancies. Consequently, new therapeutic targets and treatment approaches are needed for CRPC.

The transcription factor (TF) GATA2 has been identified as an important driver of PC, including CRPC. GATA2, one of six members of the GATA family of TFs, has been primarily implicated in driving developmental and differentiation processes, particularly in hematopoietic stem cells (Tsai *et al.* 1994, Tsai & Orkin 1997, Bresnick *et al.* 2010). GATA2 is the most highly expressed GATA family member in normal and malignant human prostate, while in the mouse, both GATA2 and GATA3 are highly expressed in the anterior and dorsal-lateral prostate lobes (Xiao *et al.* 2016). We have generated prostate-specific double *Gata2* and *Gata3* knockout (KO) mice and found that they exhibit decreased prostate-to-body weight ratio and dramatically reduced expression of the mRNAs for the AR-target genes *Probasin* and *Nkx3.1* (Xiao *et al.* 2016). In human PC cells, silencing *GATA2* results in inhibition of cell proliferation, AR expression, and AR signaling. The effects of GATA2 can be exerted at several steps of the AR signaling axis, including functioning as a pioneer factor (that facilitates AR to access chromatin and initiate transcription (Wang *et al.* 2007), inducing AR gene expression (He *et al.* 2014, Wu *et al.* 2014) and post-translationally promoting the activity of both full-length and splice-variant AR by enhancing recruitment of steroid receptor coactivators to AR (He *et al.* 2014, Zhao *et al.* 2016). AR-independent growth-promoting effects of GATA2 have also been reported (Vidal *et al.* 2015). As high GATA2 expression and transcriptional activity are linked to poor prognosis in PC (Chiang *et al.* 2014, He *et al.* 2014), and GATA2 being considered a transcriptional partner and coactivator for AR, GATA2 is poised as a promising therapeutic target for the inhibition of advanced CRPC.

We previously demonstrated that the small molecule K-7174, which has been reported to be a potential GATA inhibitor within the context of endothelial cell adhesion (Umetani *et al.* 2000), exerts anticancer activity against

GATA2-dependent PC cells (He *et al.* 2014). However, K-7174 is not being developed further by its manufacturer/patent holder, and, consequently, it has no path to the clinic. This led us to examine for agents with a structural similarity that could be used clinically. Via *in silico* screen, we identified dilazep, a drug that has been used as a vasodilator (mechanistically works as an adenosine reuptake inhibitor (Deguchi *et al.* 1997)) in patients with hypertension, cardiovascular, and renovascular disorders in Japan and several European countries (Sambhi *et al.* 1989). Our studies in PC cells demonstrate that dilazep is able to inhibit proliferation and AR signaling in both androgen-dependent cells and castration-resistant PC cell lines *in vitro* and is active in an *in vivo* patient-derived xenograft (PDX) model. We also validated, via global gene expression profiling, RT-qPCR and reporter assay, its capacity to inhibit the GATA2 transcriptional program. Dilazep suppressed the expression of AR, c-MYC, FOXM1, CENPE, EZH2, and several other PC drivers. Using cellular thermal shift assay (CETSA), ChIP-qPCR, and GATA2 DNA-binding assay, we further confirmed GATA2 target engagement by dilazep and inhibition of GATA2 recruitment to chromatin and DNA. Our findings provide proof of principle that GATA2 can be effectively targeted by small molecules in PC for therapeutic purposes.

Materials and methods

Structure-based prediction

In order to identify compounds with similar properties as K-7174, we utilized SuperPred (<https://prediction.charite.de/>), an algorithm that was designed to look for similar therapeutic compounds based on a 2D, fragment, and 3D similarity search pipeline (Nickel *et al.* 2014). The input compound is screened against 2650 drugs that have anatomical therapeutic chemical (ATC) classification codes assigned. Therefore, only those drugs can be displayed as similar drugs. The resulting score is based on the output of the similarity pipeline, which compares structural fingerprints as well as 3D structures using a superposition algorithm.

Cell culture

LNcaP cells (American Type Culture Collection (ATCC)) were cultured in RPMI-1640 (Gibco (ThermoFisher)) supplemented with 10% fetal bovine serum (FBS) (Gibco). LNcaP-Abl cells (henceforth referred to as Abl cells) (Culig *et al.* 1999) (a kind gift from Dr Zoran Culig, Innsbruck

Medical University, Innsbruck, Austria) were cultured in phenol-red free RPMI-1640 media (Gibco) supplemented with 10% charcoal-stripped serum (CSS). LNCaP MDV-3100/enzalutamide-resistant (MDVR) cells were generated by continually culturing parental LNCaP cells as previously described, with the addition of 25 μ M MDV-3100 (enzalutamide), for more than a year (enzalutamide concentration was decreased to maintenance of 10 μ M during experiments). 22Rv1 cells (ATCC) were cultured in RPMI-1640 with 10% FBS. LAPC4 cells (ATCC) were cultured in Iscove's Modified Dulbecco's Media (IMDM, Life Technologies) plus 15% FBS, 1 nM R1881, and 2 mM of L-glutamine. PC-3 cells (ATCC) were cultured in DMEM/F12 (F-12 Nutrient Medium, Life Technologies) with 10% FBS. RWPE-1 epithelial cells (ATCC) derived from the peripheral zone of a histologically normal adult human prostate and immortalized via human papilloma virus 18 were cultured in keratinocyte serum-free medium according to the instructions of ATCC. All cells culture media also contained penicillin/streptomycin (P/S; 100 units/mL; Gibco). Cells were maintained in a 37°C incubator with 5% CO₂. All cell lines were authenticated by STR fingerprinting on an annual basis and used within six passages after thawing. Cell lines were tested for mycoplasma contamination prior to experimental use.

MTT assay

Cells were seeded in 24-well plates and following 24 h of attachment treated with dilazep (Santa Cruz Biotechnologies) (or vehicle control) at the indicated concentrations for 96 h, at which point MTT (Sigma-Aldrich) was added to a final concentration of 50 μ g/mL and incubated at 37°C for 2 h. The precipitated crystals were dissolved with 92% isopropanol/8% 1 N HCl. The optical density was calculated as the difference between the absorbance at 570 nm and the absorbance at 630 nm and normalized to the respective controls.

5-Ethynyl-2'-deoxyuridine (EdU) incorporation/cell proliferation assay

22Rv1 (1×10^5 cells/well) and LNCaP cells (2.5×10^5 cells/well) were seeded in 12-well plates. The following day, the cells were treated with 0, 20, or 50 μ M dilazep for 24 h. Experiments were performed in triplicates. Before harvesting, the cells were incubated in the presence of 10 μ M EdU as a thymidine nucleoside analog for 90 min, to allow incorporation of the compound during the S-phase of a cell cycle. Newly synthesized EdU-labeled DNA was

fluorescently labeled through a click chemistry reaction with the Alexa Fluor® 488 (AF488) conjugated azide. AF488-labeled azide was reacted with the incorporated EdU according to the manufacturer protocol (Click-&-Go EdU 488 Flow Cytometry Assay Kit; Click Chemistry Tools). Cells were labeled with DAPI to evaluate DNA content. BD FACSanto flow cytometer was used for determining the percentage of S-phase cells in the population. The data were analyzed in FlowJo.

Gene expression profiling after treatment with dilazep

Cells were treated with 50 μ M dilazep for 48 h. Total RNA was extracted using Trizol (Life Technologies) and purified with the RNeasy Mini Kit (Qiagen) following the manufacturer's instructions. RNA was reverse transcribed and the microarray hybridization was performed using the Illumina Gene Expression Sentrix BeadChip HumanHT-12_V4 (Illumina) at the Laboratory for Translational Genomics at Baylor College of Medicine, as previously described (Geng *et al.* 2014). Each experimental condition (cell line/treatment) was studied in triplicate.

Gene expression profiling after treatment with siRNA

Cells were transfected with Stealth siRNA (25 nM, LifeTechnologies, ThermoFisher Scientific) against GATA2 (clone: HSS104003), or non-target control (siNT), using Lipofectamine RNAiMax (LifeTechnologies) according to the manufacturer's instructions and as previously described (He *et al.* 2014). RNA was extracted 72 h post-transfection using Trizol (LifeTechnologies) according to the manufacturer's instructions. RNA was submitted for library preparation and quantification at the Avera Institute for Human Genetics (Sioux Falls, SD), where it was processed as previously (Kaochar *et al.* 2018). Each experimental condition (cell line/treatment) was studied in triplicate.

Gene set enrichment analysis

All microarray data were normalized by using the Bioconductor lumi (Du *et al.* 2008) package using the R statistical system. Gene-expression differences were inferred using *t*-test and imposing a fold change > 1.25 or $< 1/1.25$ ($P < 0.05$). Gene set enrichment analysis (GSEA) was carried out using the GSEA software package (Subramanian *et al.* 2005) to assess the degree of similarity among the studied gene signatures, as previously described (Geng *et al.* 2014,

2017). In addition, we utilized a signature derived from genes differentially expressed between metastatic CRPC and primary, hormone-naïve PC patient specimens (Cai *et al.* 2013). We also utilized a recently described MYC/RAS co-activation signature (META-16) associated with prostate cancer metastasis (Arriaga *et al.* 2020). Moreover, we performed ingenuity pathway analysis (Qiagen). For analysis of c-MYC transcriptomic signatures in prostate models (described in detail in Geng *et al.* 2017), we used three publicly available gene expression datasets: (1) following knockdown of c-MYC via siRNA in LNCaP, DU145, and PC3 PC cells (Koh *et al.* 2011), (2) upon overexpression of c-MYC for 5 or 12 h in LNCaP cells (GSE51384 and Barfeld *et al.* 2015), and (3) upon c-MYC overexpression in epithelial cells isolated from the mouse ventral prostate (GSE37428 and Ju *et al.* 2013).

Comparison of the transcriptional program of dilazep with GATA2 activity score, AR activity score, and c-MYC activity score in PC patient cohorts

We applied the gene signature derived from treatment of LNCaP cells with dilazep, as well as the previously published footprints of GATA2 (LNCaP+GATA2 siRNA, GSE63539), AR (LNCaP+AR siRNA, GSE63539) and c-MYC (overexpression of c-MYC for 12 h in LNCaP cells (GSE51384 and Barfeld *et al.* 2015), and knockdown of c-MYC via siRNA in LNCaP (Koh *et al.* 2011)) to three previously reported cohorts of human primary PC specimens collected via prostatectomy: Taylor *et al.* (2010), Cai *et al.* (2013), and the cancer genome atlas (TCGA) (<https://tcga-data.nci.nih.gov/tcga/>). Within each dataset, we utilized the expression of each gene to calculate its respective z-score for each sample, relative to the normal prostate gland specimens available in that cohort. We computed the sum z-score for each sample (the z-scores of downregulated genes were subtracted from the z-scores of upregulated genes), as described previously (Taylor *et al.* 2010). Finally, for each pair of signatures, we plotted the cumulative z-scores on the x and y axis and computed the Pearson correlation coefficient R and associated *P*-value using the R statistical system.

Reverse phase protein array analysis

RPPA analysis was performed as previously described (Chang *et al.* 2015, Creighton & Huang 2015). Briefly, cells were grown in six-well dishes and treated with 50 μ M dilazep for 48 h. Cells were washed, lysed, quantified, and submitted to the Baylor College of Medicine Antibody-based Proteomics Core for analysis. Each lysate was run in

technical triplicates, with three biological replicates run per group. The fluorescence-labeled slides were scanned with a Molecular Devices GenePix 4400 AL and the intensity data were extracted with GenePix Pro 7.0. Intensity for each spot was obtained after subtracting the local background and group-based normalization (Chang *et al.* 2015) was used to adjust for total protein variation, background, and non-specific labeling. Subsequent statistical analysis were performed on the median of the technical triplicate in each sample. Proteins with maximum intensity less than 200 were removed from the subsequent analysis and significantly altered proteins between different experimental conditions were determined using the Student's *t*-test with *P*-value < 0.05 and fold change > 1.25 or < 1/1.25.

A complete list of antibodies used for RPPA is presented in Supplementary Table 1 (see section on [supplementary materials](#) given at the end of this article).

Immunoblotting

Cells were lysed in RIPA lysis buffer (25 mM Tris-HCl, 150 mM NaCl, 1% IGEPAL-630, 0.5% sodium deoxycholate, 0.1% SDS, 1 mM EDTA, 5% glycerol, protease inhibitor tablets (Roche), and phosphatase inhibitor tablets (Roche)). Lysates were sonicated for 1 min (BioRuptor, Diagenode (Belgium)). Total protein was quantified via Biorad DC Kit (Biorad). Total protein lysate (40 μ g) was loaded into 8.5% polyacrylamide gels or NuPage 4–12% Bis-Tris gels and transferred as previously described (He *et al.* 2014). Images were acquired using an infrared scanner (Odyssey (LiCoR), Lincoln, NE) and analyzed with the corresponding ImageStudio software (LiCoR). Antibodies used were: AR (Cell Signaling, #3202), GATA2 (Cell Signaling, #4595), GATA2 (Abclonal, #A0677), Vinculin (Santa Cruz Biotechnologies, sc-25336), c-MYC (Cell Signaling, #9402), and β -actin (Santa Cruz, sc-8432 or Invitrogen #MA1-140).

Quantitative real-time reverse transcription PCR (RT-qPCR)

RNAs were purified using Rneasy Mini Kit (Qiagen) and cDNA synthesis was performed using cDNA RT Kit (Applied Biosystems). mRNA expression was measured using a real-time detection system (Applied Biosystems StepOnePlus™) in 96-well optical plates using Perfecta™ qPCR FastMix™ (Quanta Biosciences). 18S was used as an endogenous control. The primer sequences were: CCNA2, 5'-TTGTAGGCACGGCTGCTATGCT-3' and 5'-GGTGCTCCATTCTCAGAACCTG-3'; CENPF, 5'-AGCACGACTCCAGCTACAAGGT-3'

and 5'-CATCATGCTTTGGTGTCTTTCTG-3';
AURKA, 5'-GCAACCAGTGACCTCCTCCTG-3'
and 5'-AAGTCTTCCAAAGCCCACTGCC-3';
MYC, 5'-CCTGGTGCTCCATGAGGAGAC-3' and
5'-CAGACTCTGACCTTTTGCCAGG-3'; RAD51AP1,
5'-CTTCTGGAAGGCAGTGATGGTG-3' and
5'-AGAGAAGTCTCGTCATTATCCTC-3'. All analyses were
performed in triplicate, and statistical evaluation was
performed via *t*-test.

Cellular thermal shift assay (CETSA)

To analyze the interaction between GATA2 and dilazep, CETSA was performed as described previously (Jafari *et al.* 2014), with minor modifications. Briefly, 22Rv1 cells were incubated with vehicle (DMSO) or dilazep (50 μ M) for 1 h. After treatment, cell pellets were washed and resuspended in PBS buffer containing protease and phosphatase inhibitors. The cell suspension was aliquoted into PCR tubes and heated for 3 min in the Veriti 96-well thermal cycler to 61, 64, and 67°C. Subsequently, cells were lysed by two repeated freeze-thaw cycles with liquid nitrogen. The cell lysates were briefly vortexed in the tubes and then centrifuged at 20,000 *g* for 20 mins at 4°C. The supernatant was analyzed by SDS-PAGE (25 μ L of lysate from each tube), followed by immunoblotting analysis. The protein levels of GATA2 were normalized to the corresponding levels of vinculin control for each condition.

GATA2 DNA binding assay

The DNA binding assay for GATA2 was performed using the GATA2 transcription factor activity assay kit (RayBiotech, TFEH-GATA2) and nuclear extracts from LNCaP cells (cultured in RPMI supplemented with 10% FBS and 5 nM of R1881) treated with DMSO (control) or dilazep (50 μ M or 100 μ M) for 16 h, according to manufacturer's protocol. Briefly, this assay uses a double stranded DNA-coated plate with canonical GATA2 binding sequences (GATA motif ATCWGATA (W=A/T)) to detect active GATA2 in nuclear extracts (50 μ g per well) following short incubation. Subsequently, primary antibody against GATA2 is used to recognize the GATA2-DNA complex and a HRP-conjugated secondary antibody is used for detection. After washing away any unbound antibody, signal absorbance is captured using a spectrophotometric plate reader at 450 nm. Nuclear extract was prepared using the Nuclear and Cytoplasmic Extraction Kit (NE-PER™ Nuclear and Cytoplasmic Extraction Reagents, Catalog number: 78833, ThermoFisher Scientific) according manufacturer's instructions.

GATA2 CHIP-PCR

LNCaP cells (1.5×10^7) were plated in 15 cm dishes and kept for 24 h in RPMI1640 supplemented with 10% FBS, to allow the cells to attach to the dish. Cells were treated with 5 nM R1881 and either dilazep (10 μ M) or DMSO for 16 h. Cross-linking of proteins to DNA was performed by adding formaldehyde drop-wise directly to the media to a final concentration of 1% and rotating gently at room temperature (RT) for 15 mins. Glycine was added to a final concentration of 125 mM to the media, and then cells were incubated for 5 mins at RT, followed by rinsing twice with cold PBS. Cells were scraped off in cold PBS with protease inhibitor cocktail (cOmplete™, Roche), cell suspension was transferred into 15 mL tubes and centrifuged for 5 mins at 4°C, 750 *g*. The pellet was resuspended in ChIP lysis buffer with protease inhibitors (1000 μ L PBS per 1×10^7 cells) and incubated for 10 mins on ice. Lysates were sonicated with Bioruptor Pico sonication device (Diagenode) to shear DNA to an average fragment size of 200–500 bp. Samples were diluted 1:5 with ChIP dilution buffer and incubated either with 10 μ g of GATA2 antibody (sc-9008X SantaCruz) or IgG and rotated at 4°C overnight. Next, protein A/G agarose beads (sc-2003, SantaCruz) was added to all samples and rotated for 6 h at 4°C. Samples were washed several times with various salt wash buffers. DNA was eluted using elution buffer, reverse crosslinked, and treated with RNase A and proteinase K for 1 h. Subsequently, DNA was purified using Purelink PCR cleaning kit and analyzed by real-time quantitative PCR using Power SYBR® Green PCR master mix (Applied Biosystems). Sequences of ChIP primers used: GATA2 c-MYC enh (amplified fragment chr8:127852571+127852674), forward primer: TCGTAGGGTTGGTGTGTTGAATG, reverse primer: CAAGGGCTTAACCTGCCTTAAT; KLK3 (amplified fragment chr19:50850923+50851007), forward primer: GCCTGGATCTGAGAGAGATATCATC, reverse primer: ACACCTTTTTTTTCTGGATTGTTG; gene desert (amplified fragment chr17:79882948+79883067), forward primer: TTGACTGCAGGGAGTCAGTG, reverse primer: GATTTGTGGGGGTGATGAAG.

Reporter assay

22Rv1 cells were seeded in 96-well plates (10,000 per well) in RPMI1640 with 10% FBS and incubated at 37°C, 5% CO₂, to allow attachment. Cells were transfected with a reporter vector (pGL3/PSA61-Luc (Cleutjens *et al.* 1997)) and vectors encoding for Renilla luciferase (pGL4.75, Promega) and GATA2 (pcDNA3-GATA2) using jet PRIME transfection kit (Polyplus) according to the manufacturer protocol. After

24 h, cells were treated with 5 nM R1881 and either 10 μ M dilazep or DMSO for 24 h. Luciferase activity in cells was measured with Dual-Luciferase Reporter Assay System (Promega) according to the manufacturer's protocol. In brief, after treatment, the cells were washed with PBS and lysed with 20 μ L of passive lysis buffer. Lysates were transferred into a 96-well white opaque plate, and firefly luciferase and Renilla luciferase activity was measured using SynergyH1 plate reader (Biotek). Firefly reagent was injected to each well, and after quantifying the firefly luminescence, this reaction was quenched, and the Renilla luciferase reaction was simultaneously initiated by adding Stop & Glo[®] Reagent to the same well. Subsequently, Renilla luciferase activity was measured. Firefly luciferase activity was normalized to Renilla luciferase activity in each well. Assays were performed in triplicates.

***In vivo* studies**

All animal experiments and procedures were performed in compliance with ethical regulations and the approval of the Baylor College of Medicine Institutional Animal Care and Use Committee (IACUC). Six-week-old CB17SCID (CB17/Icr-Prkdc^{scid}/IcrIcoCrl) immunodeficient male mice were purchased from Charles Rivers Laboratories (Strain code 236) and used as transplant recipients. All mice were housed in a pathogen-free animal barrier facility under constant humidity and temperature, with 12 h light:12 h darkness cycles and monitored daily. We used a PC patient-derived xenograft (PDX) model, MDA-PCa-337A, generated by Dr Nora Navone at MD Anderson Cancer Center from a liver metastasis. To establish tumors, a 3 \times 3 \times 3 mm fragment of tumor was coated in Matrigel and implanted subcutaneously into the left flank of castrated SCID mice. Treatment was initiated one day after implantation. Seven animals were used per group. Dilazep was dissolved in molecular grade water at 200 mg/mL and administered intraperitoneally at 50 mg/kg daily 5 days per week (M-F). Tumor growth was monitored weekly by caliper measurements. Mice were weighed and observed regularly throughout the study for signs of illness or distress related to tumor growth and/or drug toxicity. Statistical analysis was performed by two-way ANOVA. All mice were euthanized by CO₂ asphyxiation followed by cervical dislocation once tumors in untreated mice reached near protocol-defined tumor size limits (15 mm max diameter).

Statistical analysis

Unless otherwise indicated, statistical analysis between groups was performed via the Student's *t*-test. For the *in vivo* studies, we used two-way ANOVA.

Results

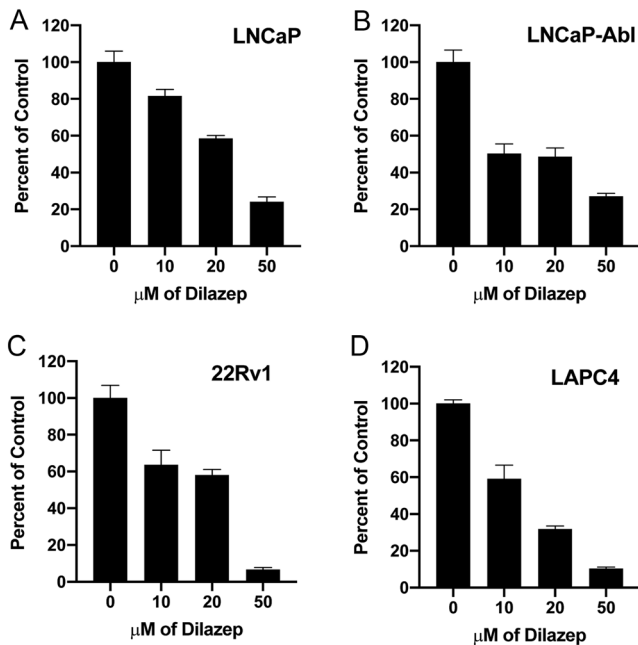
***In silico* prediction of a clinically available drug with properties similar to K-7174**

Previously, we reported K-7174 as a potent small molecule inhibitor of GATA2 driven transcriptional program in PC cells (He *et al.* 2014). Unfortunately, K-7174 has no clear path to the clinic. Thus, we screened for alternative, structurally related compounds *in silico*, using the SuperPred algorithm (<http://prediction.charite.de/>) (Nickel *et al.* 2014) and identified dilazep (C₃₁H₄₄N₂O₁₁, MW 604.7 g/mol), a vasodilator, as a clinically available drug with potential inhibitory activity against GATA2 (Supplementary Fig. 1).

Dilazep inhibits GATA2-dependent PC cell proliferation

We first examined the anticancer activity of dilazep against a panel of GATA2-dependent CRPC cell lines using MTT viability assays (Fig. 1): AR-positive, androgen-sensitive LNCaP, and LAPC4 (previously demonstrated to be GATA2-dependent (He *et al.* 2014)); AR-positive, androgen insensitive (LNCaP)-Abl and (AR-variant harboring) 22Rv1 (previously demonstrated to be GATA2-dependent (He *et al.* 2014)), and enzalutamide-resistant (MDVR) cells. The MDVR cells express higher levels of several cancer drivers compared to parental LNCaP cells (Supplementary Fig. 2), including SOX9 (an important transcription factor and CRPC driver (Wang *et al.* 2008, Ma *et al.* 2016)), YAP1 (Kuser-Abali *et al.* 2015), HER3 (Soler *et al.* 2009), phospho-Akt, SRC-3 (an important transcriptional coactivator (Zhou *et al.* 2005, Geng *et al.* 2013, Foley & Mitsiades 2016)), and EZH2 (Varambally *et al.* 2002, Bryant *et al.* 2007, Yu *et al.* 2010, Xu *et al.* 2012). MDVR cells also exhibited increased levels of LC3B/ATG3 and decreased levels of LC3A, suggesting a role for autophagy, in agreement with prior reports that increased autophagy may serve as a survival mechanism of resistance to enzalutamide (Nguyen *et al.* 2014, Kranzbuhler *et al.* 2019). MDVR cell proliferation was GATA2-dependent (Supplementary Fig. 3A) and sensitive to dilazep (Supplementary Fig. 3B). Inhibition of proliferation by dilazep was significantly lower in PC-3 and RWPE-1 cells (Supplementary Fig. 3C), both of which are AR-negative and, as we have previously demonstrated (He *et al.* 2014), GATA2-independent.

The results of the MTT assay were confirmed with the EdU incorporation assay (Supplementary Fig. 3D, E, F and G), which showed concentration-dependent inhibition of cell proliferation, evidenced by reduced percent of cells in S-phase in 22Rv1 and LNCaP cells.

**Figure 1**

Dilazep inhibits proliferation of PC cells: MTT assay in PC cell lines after treatment with increasing concentrations of dilazep (0–50 μ M) for 96 h. OD was calculated as absorbance at 570 nm – absorbance at 630 nm and normalized to the respective vehicle controls. Data are shown as average \pm s.d. The IC50 for dilazep was generally in the range of ~10–20 μ M.

Dilazep targets cell cycle-related signaling in both androgen-dependent and CRPC cell lines

In order to characterize the molecular pathways affected by dilazep in PC cells, we treated the androgen-dependent LNCaP cells, the androgen-independent Abl, and the MDV-3100-resistant MDVR cells with dilazep, followed by global gene expression analysis. GSEA of these transcriptional profiles against the Molecular Signature Database (MSigDB) revealed that the most suppressed (top enriched terms) were associated with cell cycle, mitosis, DNA replication, E2F signaling, c-MYC signaling, and DNA repair (Fig. 2A, B and Supplementary Fig. 4A). We also found suppression of gene sets related to stemness, such as the transcriptional programs of Nanog, Sox2, Oct4, and other stem cell programs (Supplementary Fig. 4B). The transcriptional signature caused by dilazep treatment (50 μ M for 48 h) was highly concordant between our three cell line models. A list of selected genes involved in cell-cycle regulation, cell survival, metabolism, DNA replication, recombination, and repair, and their fold-change (FC) in expression after dilazep treatment, are shown in Supplementary Fig. 5A. Importantly, the mRNAs for c-Myc itself, FOXM1, CENPE, EZH2, UBE2C, RRM2, and several other PC drivers were significantly suppressed by dilazep.

Confirmatory results obtained by RT-qPCR are shown in Supplementary Fig. 5B.

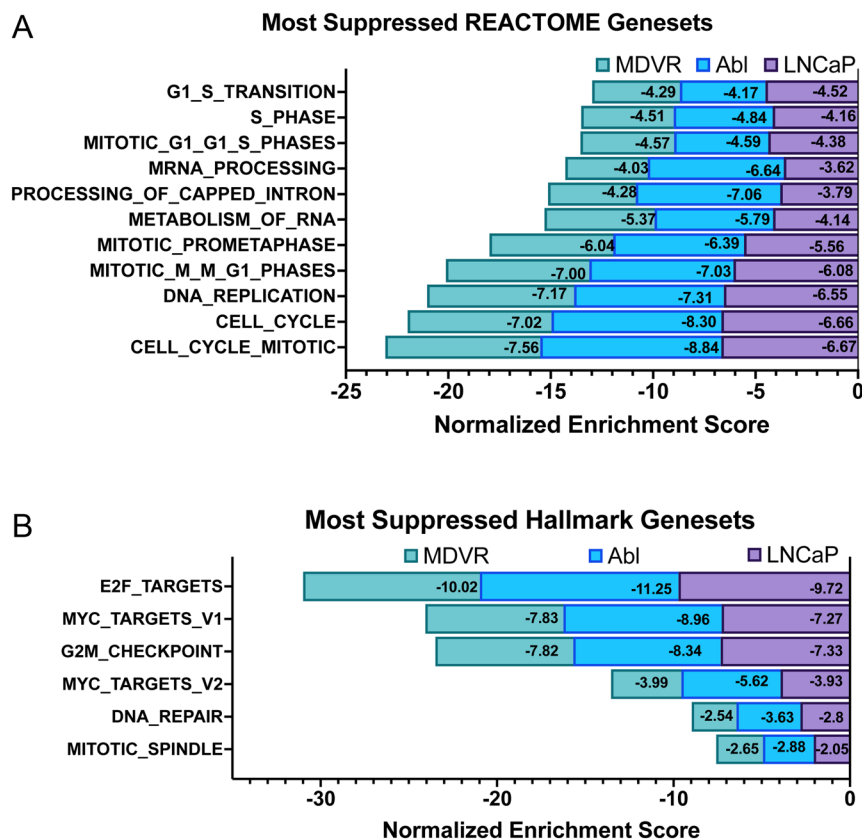
Gene expression analysis reveals that dilazep suppresses GATA2- and AR-driven signaling in PC cells

Next, we compared the transcriptional footprint of dilazep with that of GATA2 siRNA in LNCaP (GSE63539, previously reported by our group (He *et al.* 2014)), Abl, and MDVR cells (generated as part of this current study). We found that the transcriptional footprint of dilazep was strongly concordant with that of GATA2 siRNA both in androgen-dependent and castration-resistant PC cells. In each cell line, genes downregulated by GATA2 siRNA were strongly enriched among the genes suppressed by dilazep, while genes upregulated by GATA2 siRNA were strongly enriched among the genes induced by dilazep in the same cell line. This validates our bioinformatics prediction and provides evidence that dilazep indeed suppresses the GATA2 transcriptional program, in both androgen-dependent and castration-resistant PC cells (Fig. 3A).

Having previously demonstrated that GATA2 is necessary for AR expression and transcriptional activity in PC cells (He *et al.* 2014), we examined whether dilazep can inhibit AR signaling in PC cells. For that, we compared the transcriptional footprint of dilazep with that of AR siRNA in LNCaP (GSE63539, previously reported by our group (He *et al.* 2014)) and Abl (GSE11428, by Wang *et al.* 2009). We found that the transcriptional footprint of dilazep was strongly concordant with that of AR siRNA both in androgen-dependent and castration-resistant PC cells. In each cell line, genes downregulated by AR siRNA were strongly enriched among the genes suppressed by dilazep, while genes upregulated by AR siRNA were strongly enriched among the genes induced by dilazep in the same cell line. This provides evidence that dilazep indeed suppresses the AR axis, not only under androgen-dependent conditions but also in CRPC cells (Supplementary Fig. 6).

Dilazep suppresses the metastatic program of PC cells

We also compared our dilazep-derived signatures to a signature derived from genes differentially expressed between metastatic CRPC and primary, hormone-naïve PC patient specimens (Cai *et al.* 2013). Importantly, we found that genes preferentially expressed in metastatic CRPC tissues were strongly suppressed by dilazep in all three

**Figure 2**

Dilazep suppresses cell cycle and the c-MYC transcriptional program. (A) Using GSEA, we analyzed our dilazep signatures (derived from treatment with 50 μ M dilazep for 48 h) and found that, across all three PC cell lines tested, the most suppressed REACTOME gene sets were related to cell-cycle, mitosis and DNA replication. (B) Using GSEA, we analyzed our dilazep signatures and found that, across all three PC cell lines tested, the most suppressed HALLMARK gene sets were related to cell-cycle progression (E2F Targets and G2/M Checkpoint), downstream targets of c-MYC signaling (Myc Targets v1 and Myc Targets v2), and DNA Repair, highlighting dilazep as a potentially beneficial compound for inhibition of PC growth, regardless of androgen-dependence. All $P < 0.001$. A full color version of this figure is available at <https://doi.org/10.1530/ERC-21-0085>.

cell lines tested, while genes downregulated in metastatic CRPC tissues were strongly enriched among the genes induced by dilazep, supporting that dilazep suppresses the metastatic program of PC cells (Fig. 3B). Moreover, we found that dilazep suppressed, in all three lines, a recently described MYC/RAS co-activation signature (META-16) (Arriaga *et al.* 2020) that is associated with prostate cancer metastasis (Fig. 3B).

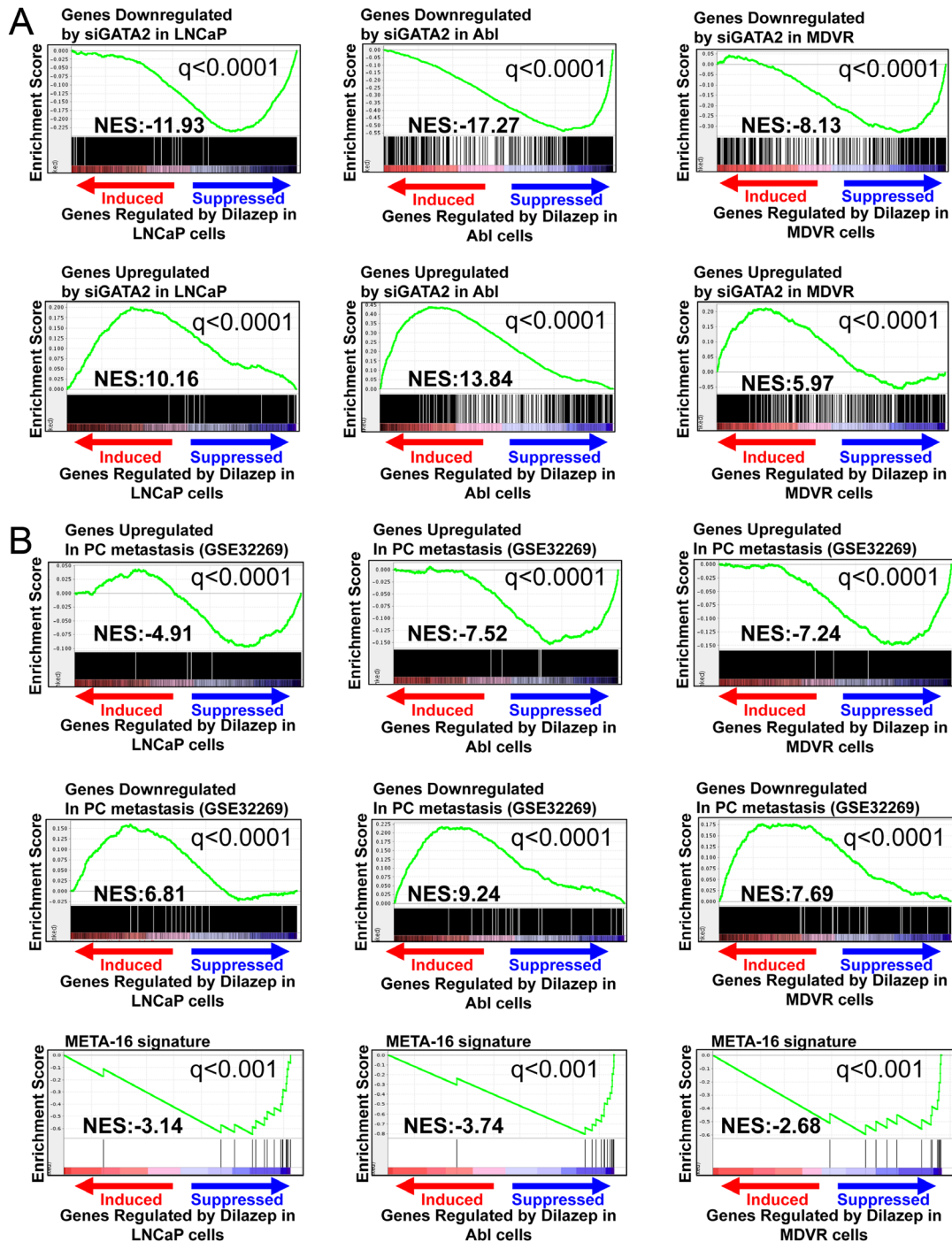
Dilazep suppresses the c-MYC transcriptional program in PC cells

Our HALLMARK results (Fig. 2B) highlighted that c-MYC signaling is blocked by dilazep. Moreover, ingenuity pathway analysis revealed that the top (most inhibited) upstream regulator in the dilazep signatures is the c-MYC pathway. In order to further validate these observations, we next compared our signatures of dilazep treatment of our three PC cell lines against several publicly available prostate-specific signatures of c-MYC activity: (1) following knockdown of c-MYC via siRNA in LNCaP, DU145, and PC3 PC cells (Koh *et al.* 2011), (2) upon overexpression of c-MYC for 5 or 12 h in LNCaP cells (GSE51384 and Barfeld *et al.* 2015), and (3) upon c-MYC overexpression in epithelial

cells isolated from the mouse ventral prostate (GSE37428 and Ju *et al.* 2013). In all three of our PC cell lines, dilazep suppressed gene sets upregulated by c-MYC in prostate models and induced gene sets suppressed by c-MYC, highlighting that dilazep potently blocked the c-MYC program (Fig. 4A).

The dilazep transcriptional program correlates with decreased GATA2 activity score, AR activity score, and Myc activity score in PC patient cohorts

We applied the gene signature derived from our treatment of LNCaP cells with dilazep, as well as the previously published footprints of GATA2 (GSE63539 and He *et al.* (2014)), AR (GSE63539 and He *et al.* (2014)) and c-MYC (two signatures, one from overexpression of c-MYC for 12 h in LNCaP cells (GSE51384 and Barfeld *et al.* (2015)) and the other from knockdown of c-MYC via siRNA in LNCaP Koh *et al.* (2011)), and computed an activity score for each specimen in multiple previously reported human PC specimen cohorts: Taylor *et al.* (2010), Cai *et al.* (2013), and the Cancer Genome Atlas (TCGA) (<https://tcga-data.nci.nih.gov/tcga/>). Within each human PC dataset, we found significant inverse correlation between dilazep scores and GATA2, AR,

**Figure 3**

(A) Dilazep suppresses GATA2-driven signaling in PC cells. We compared, via GSEA, the transcriptional footprint of dilazep (50 μ M for 48 h) with that of GATA2 siRNA in LNCaP, Abl, and MDVR cells. In each cell line, genes downregulated by GATA2 siRNA were strongly enriched among the genes suppressed by dilazep, while genes upregulated by GATA2 siRNA were strongly enriched among the genes induced by dilazep in the same cell line. This provides evidence that dilazep indeed suppresses that GATA2 transcriptional program, in both androgen-dependent and castration-resistant PC cells. (B) Dilazep suppresses the metastatic program of PC cells. We compared, via GSEA, our dilazep-derived signatures in LNCaP, Abl, and MDVR cells to a signature derived from genes differentially expressed between metastatic CRPC and primary, hormone-naïve PC patient specimens. We found that genes preferentially expressed in metastatic CRPC tissues were strongly suppressed by dilazep in all three cell lines tested, while genes downregulated in metastatic CRPC tissues were strongly enriched among the genes induced by dilazep, supporting that dilazep suppresses the metastatic program of PC cells. Moreover, we found that dilazep suppressed, in all three lines tested, a recently described MYC/RAS co-activation signature (META-16) (Arriaga *et al.* 2020) that is associated with prostate cancer metastasis. A full color version of this figure is available at <https://doi.org/10.1530/ERC-21-0085>.

and c-MYC activity scores, providing further evidence that dilazep suppresses the GATA2, AR, and c-MYC programs (Fig. 4B).

Dilazep suppresses protein expression of key cell-cycle regulators in androgen-dependent and CRPC cells

Having found transcriptional enrichments for cell cycle and c-MYC regulation in our dilazep-treated cells, we proceeded to protein level analysis using RPPA and immunoblotting. We assessed the effects of dilazep on LNCaP, Abl, and LNCaP-MDVR cells through RPPA. The proteomic signature caused by dilazep treatment was highly concordant between our three cell line models. The protein levels of AR and c-MYC were decreased across all three cell lines. We also found that dilazep suppressed the expression of several other PC drivers and cell-cycle regulators, including EZH2, RRM2, phospho-Rb, as well as several mediators of DNA damage repair such as BRCA1 and CHK2. Dilazep also suppressed, in at least one cell line, the protein expression of WNT5A, SOX9, AURKA,

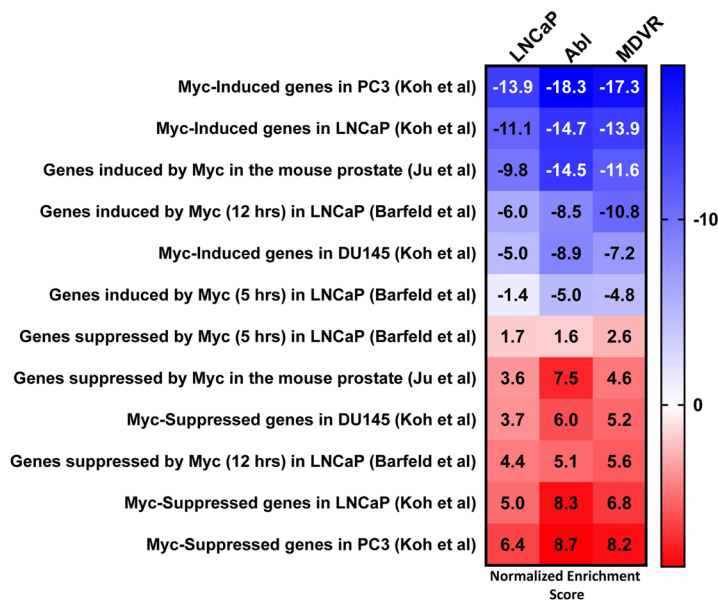
STAT5A, and the AR coactivators SRC-2 and SRC-3 (Fig. 5 and Supplementary Fig. 7).

To further expand these proteomic findings to additional cell line models, we treated 22Rv1 and LAPC4 cells with dilazep and assessed effects on protein expression of AR and c-MYC by immunoblotting (we also used LNCaP cells for continuity with the RPPA studies). Across all three cell lines, dilazep treatment dramatically decreased the protein levels of AR (including AR variants in 22Rv1 cells) and c-MYC in a dose-dependent manner (Fig. 6).

GATA2 target engagement by dilazep

Following our gene expression studies, which demonstrated profound suppression of GATA2/AR transcriptional program by dilazep, we utilized cellular thermal shift assay (CETSA) to investigate the GATA2 target occupancy by dilazep. CETSA is a broadly applicable biophysical technique allowing detection of changes in ligand/drug binding interactions directly in intact cells. The technique is based on the thermal shift

A



B

	AR Activity (per signature from GSE63539)		Myc Activity (per signature from GSE51384)		Myc Activity (per signature from Koh et al)		GATA2 Activity (per signature from GSE63539)	
	R	p-value	R	p-value	R	p-value	R	p-value
Taylor et al dataset (Primary tumors)	-0.303	0.000531	-0.323	0.000209	-0.219	0.013391	-0.584	5.73E-13
TCGA	-0.683	1.51E-39	-0.649	1.11E-34	-0.650	9.99E-35	-0.799	8.23E-63
Cai et al dataset (Primary tumors)	-0.763	3.64E-05	-0.755	4.92E-05	-0.532	0.010823	-0.820	2.96E-06

Figure 4

(A) Dilazep suppresses the c-MYC transcriptional program. Using GSEA, we compared our signatures of dilazep treatment in our three PC cell lines against publicly available prostate-specific signatures of c-MYC activity. We found that the gene programs induced by c-MYC are strongly suppressed by dilazep in all three cell lines for, while genes suppressed by c-MYC are strongly induced by dilazep. These results demonstrate that dilazep potently suppresses c-MYC activity in PC cells. All $P < 0.001$. (B) The dilazep transcriptional program correlates with decreased GATA2 activity score, AR activity score, and c-MYC activity score in PC patient cohorts. We applied the gene signature derived from our treatment of LNCaP cells with dilazep, as well as the previously published footprints of GATA2 (GSE63539 and He *et al.* 2014), AR (GSE63539 and He *et al.* 2014) and c-MYC (two signatures, one from overexpression of c-MYC for 12 hrs in LNCaP cells (GSE51384 and Barfeld *et al.* 2015) and the other from knockdown of c-MYC via siRNA in LNCaP (Koh *et al.* 2011)), and computed an activity score for each specimen in multiple previously reported human PC specimen cohorts: Taylor *et al.* (2010), Cai *et al.* (2013), and the Cancer Genome Atlas (TCGA) (<https://tcga-data.nci.nih.gov/tcga/>). Within each human PC dataset, we found significant inverse correlation between dilazep scores and GATA2, AR and c-MYC activity scores, suggesting that dilazep suppresses GATA2, AR and c-MYC activity. A full color version of this figure is available at <https://doi.org/10.1530/ERC-21-0085>.

assay (TSA) concept where ligand binding affects protein stability. We treated PC cells with 50 μM of dilazep or DMSO for 1 h and obtained nuclear fraction from various conditions. Following a heating step, which causes protein denaturing and therefore precipitation, the remaining soluble fractions (i.e. folded proteins) were isolated and analyzed by immunoblotting. The levels of GATA2 were quantified and vinculin served as control. We observed that GATA2 became less stable following dilazep treatment ($T_m = 64\text{--}67^\circ\text{C}$) compared to DMSO control in four independent experiments (Fig. 7A and B). To further confirm direct inhibition of GATA2 function by dilazep, we next performed a GATA2 DNA binding assay. Double-stranded oligonucleotides

corresponding to GATA2 consensus DNA binding sequences were immobilized on plates and incubated with lysates from PC cells treated with DMSO or dilazep (Fig. 7C). Following dilazep treatment (50 or 100 μM of dilazep for 16 h), we observed significant reduction in GATA2 binding (Fig. 7D).

We also performed ChIP-qPCR in PC cells following dilazep treatment. We examined GATA2 binding at two genomic loci: one located near the KLK3/PSA gene and a second located near c-MYC. We observed significant reduction in GATA2 binding following dilazep treatment (Fig. 8A). Of note, treatment with dilazep at this concentration and duration does not lower GATA2 protein levels (Supplementary Fig. 8). To further examine

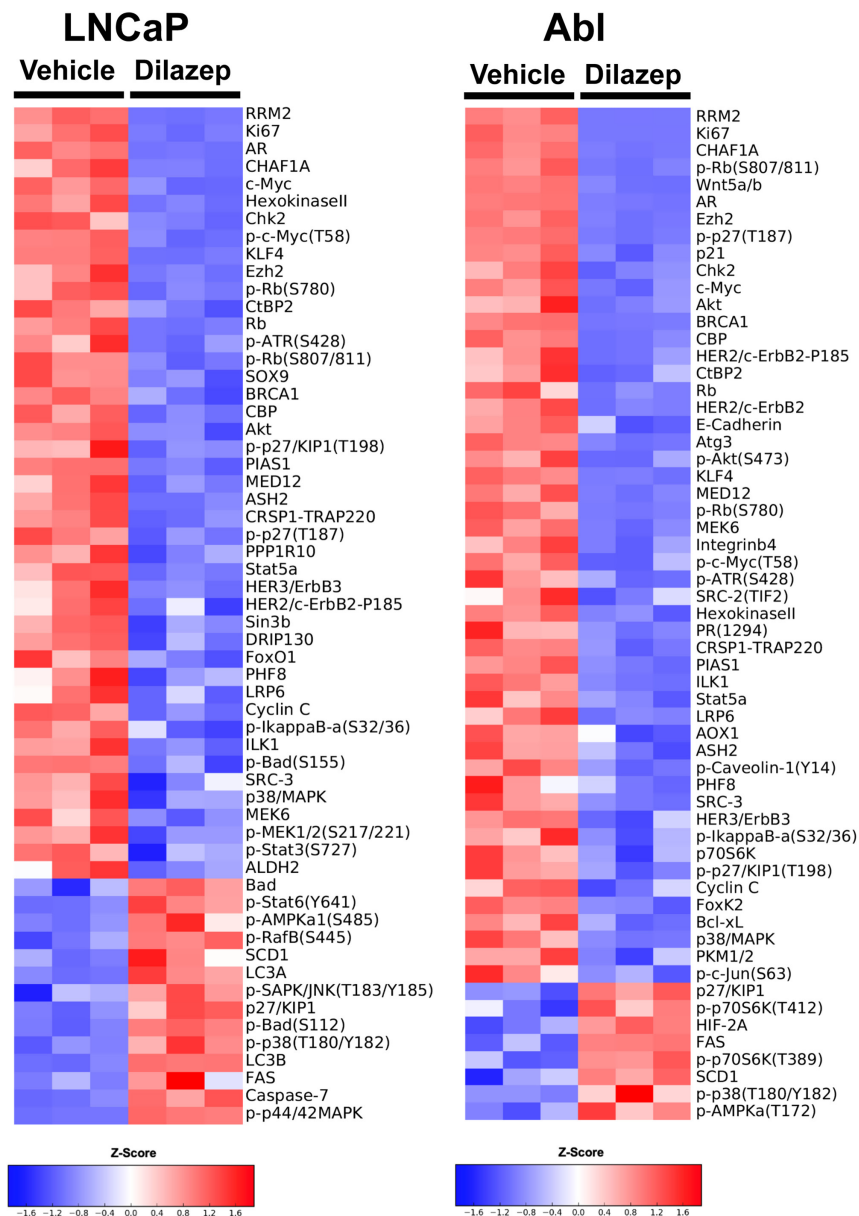


Figure 5

Dilazep treatment suppresses protein expression of AR, c-MYC, and other regulators of cell-cycle progression in LNCaP and Abl cells. The heatmap demonstrates the \log_2 -based fold-change of protein expression, documented by RPPA analysis, for dilazep-treated cells compared to vehicle-treated cells. The proteomic signature caused by dilazep treatment was highly concordant between these two cell line models, as well as with LNCaP-MDVR cells (shown in Supplementary Fig. 7). A full color version of this figure is available at <https://doi.org/10.1530/ERC-21-0085>.

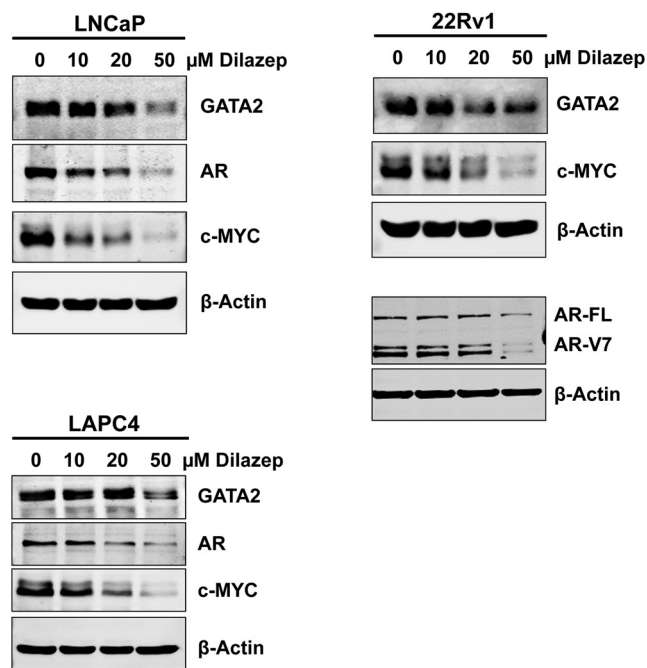


Figure 6
Immunoblotting for GATA2, AR, and c-MYC in LNCaP, 22Rv1, and LAPC4 cell treated with dilazep (0–50 μ M) for 72 h.

the functional consequences of reduced GATA2 binding at the KLK3/PSA gene, we next utilized a reporter plasmid carrying a 6-kb fragment of the promoter/enhancer region of the PSA/KLK3 gene. This fragment harbors a 440-bp regulatory region (Cleutjens *et al.* 1997) which contains three GATA2 binding motifs and one ARE. Two additional AREs and several GATA2 binding motifs are also present on this plasmid further downstream, prior to the luciferase gene (Supplementary Text file). We observed significant reduction in transcriptional output as measured by luciferase activity following dilazep treatment (Fig. 8B). Together these series of experiments strongly indicate an on-target inhibition of GATA2 by dilazep.

***In vivo* studies**

The CRPC PDX model, MDA-PCa-337A, generated by Dr Nora Navone at MD Anderson Cancer Center from a liver metastasis, was grown in castrated SCID male mice. Dilazep, dissolved in molecular grade water at 200 mg/mL and administered intraperitoneally at 50 mg/kg daily 5 days per week (M–F), inhibited PDX growth (Fig. 9A), without causing loss of animal weight (Fig. 9B).

Discussion

Novel therapeutic targets are needed in CRPC, in order to improve patient outcomes. GATA2 is an important PC and CRPC driver (Perez-Stable *et al.* 2000, Bohm *et al.* 2009, Chiang *et al.* 2014, He *et al.* 2014, Wu *et al.* 2014, Vidal *et al.* 2015, Chaytor *et al.* 2019). However, pharmacologic targeting of GATA2 is hindered by the lack of a ligand-binding pocket or an actionable site of protein activation and by the absence of an established 3-dimensional structure for the full-length GATA2.

In the present study, we predicted bioinformatically the vasodilator dilazep to be a GATA2 inhibitor. We proceeded to validate the effect of dilazep on GATA2 using CETSA (an indirect assay of target engagement) and also found that dilazep inhibits GATA2 recruitment to chromatin and DNA (using ChIP-qPCR and a GATA2 DNA-binding assay, respectively) and activity in a reporter assay. Importantly, dilazep exerted anticancer activity against GATA2-dependent (both androgen-dependent and androgen-independent) PC cell lines, while its effect on proliferation of PC-3 and RWPE-1 cells was minimal and only at high concentration. The latter finding is in agreement with our prior report that the AR-negative PC-3 cells and benign prostate cell models such as the RWPE-1 cells are resistant to GATA2 targeting via siRNA and a different small molecule inhibitor (He *et al.* 2014). Dilazep was also active against a CRPC PDX model *in vivo*, without causing mouse weight loss or apparent toxicity. Using protein and RNA profiling, we established that dilazep suppresses transcriptional programs associated with cell cycle, mitosis, DNA replication, DNA repair, E2F, and c-MYC targets in PC cells (including CRPC cells). Several cell regulators were suppressed concordantly across our cell line panel, including Ki67, p-Rb(S807/811), cyclins, and members of the CENP family.

In addition, our global gene expression profiling and confirmatory RT-qPCR studies established, for the first time, that a small molecule can suppress the GATA2 transcriptional profile. GSEA revealed that the transcriptional footprint of dilazep strongly matched that caused by GATA2 siRNA profile in all three PC cell lines, both as far as the upregulated and the downregulated genes. Application of the dilazep signature to patient samples also showed that it is associated with decreased activity of GATA2. Moreover, GSEA demonstrated that dilazep strongly matched the transcriptional footprint caused by AR siRNA in both androgen-dependent LNCaP cells and androgen-independent Abl cells.

In further exploration of this effect, we found that dilazep suppressed expression of AR itself across a wide panel of PC cell lines, including the androgen-dependent LNCaP and LAPC4 cells, the androgen-independent Abl, the enzalutamide-resistant MDVR, and the AR variant(+) 22Rv1 cells. This validates our hypothesis that pharmacological targeting of GATA2 can serve as a surrogate mechanism to inhibit AR, which is of particular importance in CRPC expressing AR variants that are resistant to enzalutamide and abiraterone.

Moreover, our GSEA revealed, using a wide variety of c-MYC-driven signatures, that c-MYC signaling was a target of dilazep in all three PC cell lines. In agreement, we found very potent suppression of c-MYC mRNA

(Supplementary Fig. 5) and protein expression (Fig. 5 and Supplementary Figs 6, 7) by dilazep in all PC cell lines tested. Application of the dilazep signature to patient samples also showed that it is associated with decreased transcriptional activity of c-MYC. Collectively, our findings suggests that c-MYC expression and function are highly GATA2-dependent in PC cells, and extremely sensitive to GATA2 inhibition, thus providing an opportunity to effectively silence the expression of an otherwise undruggable major driver of PC (Buttayan *et al.* 1987, Bernard *et al.* 2003, Edwards *et al.* 2003, Ellwood-Yen *et al.* 2003).

Dilazep also suppressed the expression of several other well-known PC drivers (Fig. 5 and Supplementary

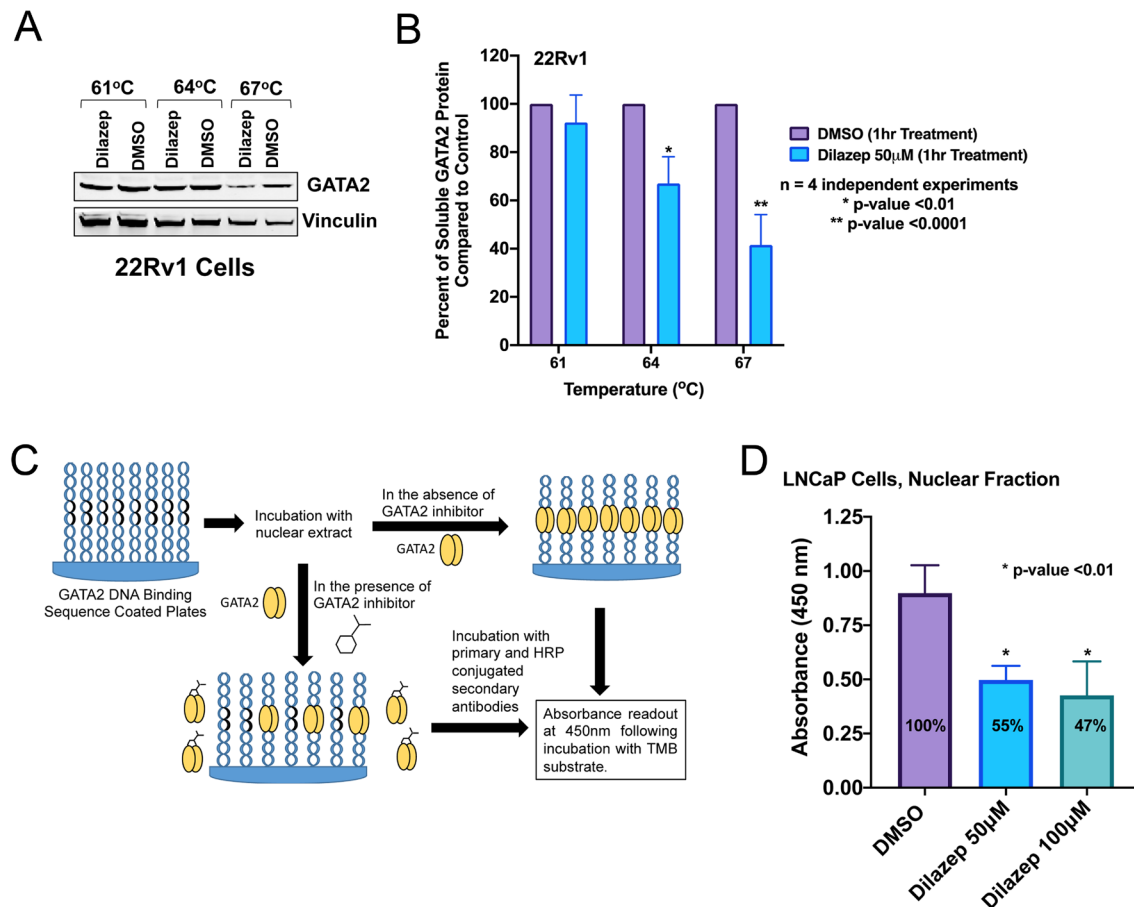


Figure 7

(A and B) Dilazep treatment resulted in destabilization of GATA2 protein. (A) Cellular thermal shift assay was performed in 22Rv1 cells following treatment with 50 µM of dilazep or DMSO for 1 h (described in 'Materials and methods'). Immunoblotting was carried out for GATA2. Vinculin served as control. A representative example (out of four independent experiments) is shown here. (B) Relative amounts of GATA2 to vinculin in dilazep-treated vs DMSO-treated samples were plotted from four independent experiments as the average ± s.d. These data support GATA2 target engagement by dilazep. (C and D) Dilazep inhibits GATA2 recruitment to DNA. (C) Schematic overview of the GATA2 DNA binding assay. (D) Nuclear extracts were prepared from LNCaP cells following treatment with DMSO (control) or dilazep (50 and 100 µM) for 16 h. DNA binding assay was performed with 50 µg of nuclear extract per well, as depicted above in C. GATA2 binding to its consensus DNA sequence was measured as described in Methods. Data from three independent experiments were plotted as the average ± s.d. All bar plots were generated using GraphPad Prism 8. A full color version of this figure is available at <https://doi.org/10.1530/ERC-21-0085>.

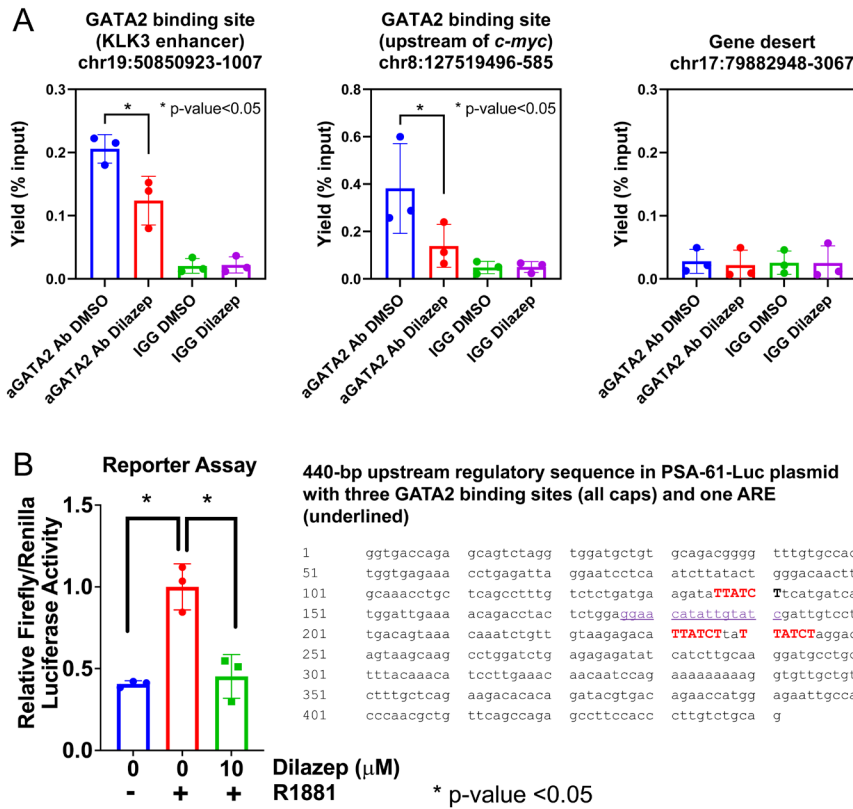


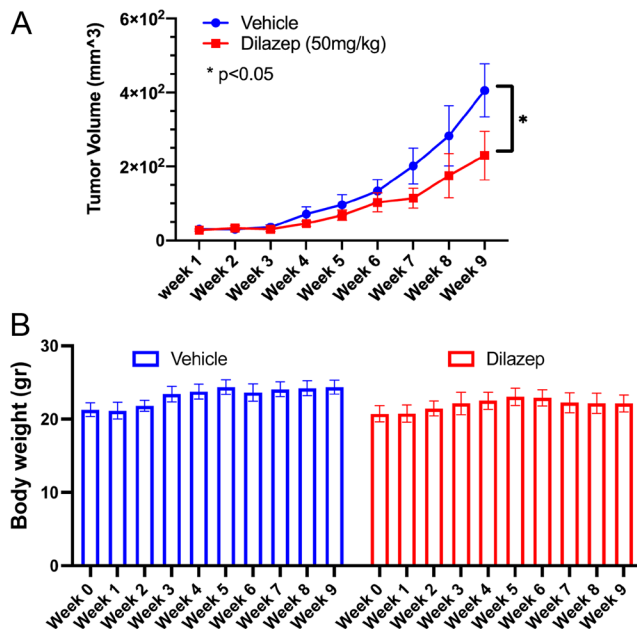
Figure 8

(A) Dilazep inhibits GATA2 recruitment to chromatin. LNCaP cells were treated with 10 μM of dilazep for 16 h and subjected to chromatin immunoprecipitation quantitative PCR (ChIP-qPCR) analysis for the presence of GATA2 on chromatin. Chromatin was fixed with formaldehyde, then DNA was extracted and sonicated into short fragments. GATA2-associated DNA was immunoprecipitated using anti-GATA2 or rabbit IgG as a negative control and analyzed by quantitative PCR as per Materials and methods. We selected two GATA2 binding sites based on prior GATA2 ChIP-seq profiles. The genomic coordinates for these sites are as indicated. Both sites harbor GATA2 binding sequences. Error bars indicate standard deviations for triplicates. (B) Dilazep suppresses transcriptional activity in a reporter assay based on the KLK3/PSA gene promoter/enhancer. 22Rv1 cells were transfected with reporter vector (pGL3/PSA61-Luc) and vectors encoding for Renilla luciferase (pGL4.75, Promega) and GATA2 (pcDNA3-GATA2) using jet PRIME transfection kit (Polyplus) according to the manufacturer's protocol. The pGL3/PSA61-Luc harbors several GATA2 binding sites (those within a 440-bp regulatory sequence are shown here; for more details, please see Supplementary Text file) and three AREs (one of which is highlighted; two additional AREs are located right before the luciferase gene start site, please see Supplementary Text file). After 24 h, cells were treated with 5nM R1881 and either 10 μM dilazep or DMSO for 24 h. Luciferase activity in cells was measured with Dual-Luciferase Reporter Assay System (Promega) according to the manufacturer protocol. Relative firefly-to-Renilla luciferase activity from three independent experiments was plotted as the means ± s.d. All bar plots were generated using GraphPad Prism 8. A full color version of this figure is available at <https://doi.org/10.1530/ERC-21-0085>.

Figs 5, 7), including FOXM1 (Aytes *et al.* 2014, Lin *et al.* 2016), CENPF (Aytes *et al.* 2014, Lin *et al.* 2016), EZH2 (Varambally *et al.* 2002, Bryant *et al.* 2007, Xu *et al.* 2012, Dardenne *et al.* 2016), UBE2C (Wang *et al.* 2009, 2011, Chen *et al.* 2011), RRM2 (Mazzu *et al.* 2019), as well as several mediators of DNA damage repair such as BRCA1 and CHK2. Dilazep also suppressed, in at least one cell line, the AR coactivators SRC-2 and SRC-3 and the PC drivers WNT5A/B, SOX9, AURKA, and STAT5A. Moreover, dilazep suppressed genes of the NANOG, SOX2, and OCT4 stem cell transcriptional programs, which are known to play important roles in PC (Gu *et al.* 2007, Sotomayor *et al.* 2009, Jeter *et al.* 2011, 2016, Chu *et al.* 2014, Kregel *et al.* 2014, Jiang *et al.* 2016, Hepburn *et al.* 2019, Sanchez *et al.* 2020, Zadvornyi *et al.* 2020).

Having discovered this capacity of dilazep to suppress several well-known PC drivers, we propose that GATA2 inhibition would be expected to affect several hallmarks of cancer. In agreement, the transcriptional program triggered by dilazep was associated with suppression of metastasis-associated genes (Fig. 3B). This supports that dilazep suppresses the metastatic program of PC cells and is in agreement with our prior findings that GATA2 expression is higher in metastatic PC compared to primary PC human specimens and also is associated with higher risk of recurrence after prostatectomy (He *et al.* 2014).

In conclusion, our study provides proof of principle that a small molecule can inhibit the GATA2 and c-MYC transcriptional programs in PC cells and can exert

**Figure 9**

The CRPC PDX model, MDA-PCa-337A, generated by Dr Nora Navone at MD Anderson Cancer Center from a liver metastasis, was grown in castrated SCID male mice. Dilazep treatment, dissolved in molecular grade water at 200 mg/mL and administered intraperitoneally at 50 mg/kg daily 5 days per week (M–F), inhibited PDX growth (A, $P < 0.05$ by two-way ANOVA), without causing loss of animal weight (B). Average values \pm s.d. are shown. A full color version of this figure is available at <https://doi.org/10.1530/ERC-21-0085>.

anticancer effects *in vitro* and *in vivo*. The ability of a GATA2 inhibitor to suppress several AR-mediated and AR-independent PC driver pathways and to overcome resistance to hormonal therapy opens new treatment opportunities for CRPC patients.

Supplementary materials

This is linked to the online version of the paper at <https://doi.org/10.1530/ERC-21-0085>.

Declaration of interest

The authors declare that there is no conflict of interest that could be perceived as prejudicing the impartiality of the research reported.

Funding

This work was also supported by the American Cancer Society RSG-14-218-01-TBG (to N M), the Prostate Cancer Foundation (S K, C C and N M), NIH 5T32CA174647-03 (S K), Department of Defense Congressionally Directed Medical Research Programs/Prostate Cancer Research Program Idea Development Awards W81XWH-15-1-0674, W81XWH-17-1-0298 and W81XWH-18-1-0288, National Cancer Institute Grant U54-CA233223 (S K and N M), the Cancer Prevention & Research Institute of Texas (CPRIT) award RP150648, the Terry Fox Foundation, the Sidney Kimmel Foundation, the Elsa U. Pardee Foundation and SPORE P50CA58183 and P50CA186784 (N M). The authors also would like to acknowledge the assistance of the Dan L. Duncan Cancer Center Shared Resources, in particular the Antibody-

based Proteomics Core/Shared Resource (supported by the NCI Cancer Center Support Grant P30CA125123). This work was also supported in part by NIH S10 instrument award (S10OD028648, SH), CPRIT Proteomics & Metabolomics Core Facility Support Award (RP170005 & RP210227) (K R, S H, C C), CPRIT Award RP150648, RP200504 (CPRIT Epigenomic Core), and NIEHS grants 1P30ES030285 and 1P42ES027725. We thank Ms Fuli Jia and Dr Danli Wu from the Antibody-based Proteomics Core/Shared Resource for their excellent technical assistant in performing RPPA experiments. This project was supported by the Cytometry and Cell Sorting Core at Baylor College of Medicine with funding from the CPRIT Core Facility Support Award (CPRIT-RP180672), the NIH (P30 CA125123 and S10 RR024574) and the expert assistance of Joel M Sederstrom.

Acknowledgements

The authors acknowledge all members of the Kaochar and the Mitsiades lab for stimulating discussions during the preparation of this manuscript. The authors also acknowledge the joint participation by Adrienne Helis Malvin Medical Research Foundation through its direct engagement in the continuous active conduct of medical research in conjunction with Baylor College of Medicine. The authors are grateful to Drs Angelo De Marzo and Stefan J Barfeld for sharing with us the fastq files from their microarrays for our analysis of the c-MYC transcriptional program.

References

- Arriaga JM, Panja S, Alshalalfa M, Zhao J, Zou M, Giacobbe A, Madubata CJ, Yeji Kim J, Rodriguez A, Coleman I, *et al.* 2020 A MYC and RAS co-activation signature in localized prostate cancer drives bone metastasis and castration resistance. *Nature Cancer* **1** 1082–1096. (<https://doi.org/10.1038/s43018-020-00125-0>)
- Aytes A, Mitrofanova A, Lefebvre C, Alvarez MJ, Castillo-Martin M, Zheng T, Eastham JA, Gopalan A, Pienta KJ, Shen MM, *et al.* 2014 Cross-species regulatory network analysis identifies a synergistic interaction between FOXM1 and CENPF that drives prostate cancer malignancy. *Cancer Cell* **25** 638–651. (<https://doi.org/10.1016/j.ccr.2014.03.017>)
- Barfeld SJ, Fazli L, Persson M, Marjavaara L, Urbanucci A, Kaukoniemi KM, Rennie PS, Ceder Y, Chabes A, Visakorpi T, *et al.* 2015 Myc-dependent purine biosynthesis affects nucleolar stress and therapy response in prostate cancer. *Oncotarget* **6** 12587–12602. (<https://doi.org/10.18632/oncotarget.3494>)
- Bernard D, Poutier-Manzanedo A, Gil J & Beach DH 2003 Myc confers androgen-independent prostate cancer cell growth. *Journal of Clinical Investigation* **112** 1724–1731. (<https://doi.org/10.1172/JCI19035>)
- Bohm M, Locke WJ, Sutherland RL, Kench JG & Henshall SM 2009 A role for GATA-2 in transition to an aggressive phenotype in prostate cancer through modulation of key androgen-regulated genes. *Oncogene* **28** 3847–3856. (<https://doi.org/10.1038/onc.2009.243>)
- Bresnick EH, Lee HY, Fujiwara T, Johnson KD & Keles S 2010 GATA switches as developmental drivers. *Journal of Biological Chemistry* **285** 31087–31093. (<https://doi.org/10.1074/jbc.R110.159079>)
- Bryant RJ, Cross NA, Eaton CL, Hamdy FC & Cunliffe VT 2007 EZH2 promotes proliferation and invasiveness of prostate cancer cells. *Prostate* **67** 547–556. (<https://doi.org/10.1002/pros.20550>)
- Buttayan R, Sawczuk IS, Benson MC, Siegal JD & Olsson CA 1987 Enhanced expression of the c-myc protooncogene in high-grade human prostate cancers. *Prostate* **11** 327–337. (<https://doi.org/10.1002/pros.2990110405>)
- Cai C, Wang H, He HH, Chen S, He L, Ma F, Mucci L, Wang Q, Fiore C, Sowalsky AG, *et al.* 2013 ERG induces androgen receptor-mediated regulation of SOX9 in prostate cancer. *Journal of Clinical Investigation* **123** 1109–1122. (<https://doi.org/10.1172/JCI66666>)
- Chang CH, Zhang M, Rajapakshe K, Coarfa C, Edwards D, Huang S & Rosen JM 2015 Mammary stem cells and tumor-initiating cells are more resistant to apoptosis and exhibit increased DNA repair activity

- in response to DNA damage. *Stem Cell Reports* **5** 378–391. (<https://doi.org/10.1016/j.stemcr.2015.07.009>)
- Chaytor L, Simcock M, Nakjang S, Heath R, Walker L, Robson C, Jones D & Gaughan L 2019 The pioneering role of GATA2 in androgen receptor variant regulation is controlled by bromodomain and extraterminal proteins in castrate-resistant prostate cancer. *Molecular Cancer Research* **17** 1264–1278. (<https://doi.org/10.1158/1541-7786.MCR-18-1231>)
- Chen Z, Zhang C, Wu D, Chen H, Rorick A, Zhang X & Wang Q 2011 Phospho-MED1-enhanced UBE2C locus looping drives castration-resistant prostate cancer growth. *EMBO Journal* **30** 2405–2419. (<https://doi.org/10.1038/emboj.2011.154>)
- Chiang YT, Wang K, Fazli L, Qi RZ, Gleave ME, Collins CC, Gout PW & Wang Y 2014 GATA2 as a potential metastasis-driving gene in prostate cancer. *Oncotarget* **5** 451–461. (<https://doi.org/10.18632/oncotarget.1296>)
- Chu GC, Zhou HE, Wang R, Rogatko A, Feng X, Zayzafoon M, Liu Y, Farach-Carson MC, You S, Kim J, *et al.* 2014 RANK- and c-Met-mediated signal network promotes prostate cancer metastatic colonization. *Endocrine-Related Cancer* **21** 311–326. (<https://doi.org/10.1530/ERC-13-0548>)
- Cleutjens KB, van der Korput HA, van Eekelen CC, van Rooij HC, Faber PW & Trapman J 1997 An androgen response element in a far upstream enhancer region is essential for high, androgen-regulated activity of the prostate-specific antigen promoter. *Molecular Endocrinology* **11** 148–161. (<https://doi.org/10.1210/mend.11.2.9883>)
- Creighton CJ & Huang S 2015 Reverse phase protein arrays in signaling pathways: a data integration perspective. *Drug Design, Development and Therapy* **9** 3519–3527. (<https://doi.org/10.2147/DDDT.S38375>)
- Culig Z, Hoffmann J, Erdel M, Eder IE, Hobisch A, Hittmair A, Bartsch G, Utermann G, Schneider MR, Parczyk K, *et al.* 1999 Switch from antagonist to agonist of the androgen receptor bicalutamide is associated with prostate tumour progression in a new model system. *British Journal of Cancer* **81** 242–251. (<https://doi.org/10.1038/sj.bjc.6690684>)
- Dardenne E, Beltran H, Benelli M, Gayvert K, Berger A, Puca L, Cyrta J, Sboner A, Noorzad Z, MacDonald T, *et al.* 2016 N-Myc induces an EZH2-mediated transcriptional program driving neuroendocrine prostate cancer. *Cancer Cell* **30** 563–577. (<https://doi.org/10.1016/j.ccell.2016.09.005>)
- Deguchi H, Takeya H, Wada H, Gabazza EC, Hayashi N, Urano H & Suzuki K 1997 Dilazep, an antiplatelet agent, inhibits tissue factor expression in endothelial cells and monocytes. *Blood* **90** 2345–2356.
- Du P, Kibbe WA & Lin SM 2008 Lumi: a pipeline for processing Illumina microarray. *Bioinformatics* **24** 1547–1548. (<https://doi.org/10.1093/bioinformatics/btn224>)
- Edwards J, Krishna NS, Witton CJ & Bartlett JM 2003 Gene amplifications associated with the development of hormone-resistant prostate cancer. *Clinical Cancer Research* **9** 5271–5281.
- Ellwood-Yen K, Graeber TG, Wongvipat J, Iruela-Arispe ML, Zhang J, Matusik R, Thomas GV & Sawyers CL 2003 Myc-driven murine prostate cancer shares molecular features with human prostate tumors. *Cancer Cell* **4** 223–238. ([https://doi.org/10.1016/s1535-6108\(03\)00197-1](https://doi.org/10.1016/s1535-6108(03)00197-1))
- Foley C & Mitsiades N 2016 Moving beyond the androgen receptor (AR): targeting AR-interacting proteins to treat prostate cancer. *Hormones and Cancer* **7** 84–103. (<https://doi.org/10.1007/s12672-015-0239-9>)
- Geng C, He B, Xu L, Barbieri CE, Eedunuri VK, Chew SA, Zimmermann M, Bond R, Shou J, Li C, *et al.* 2013 Prostate cancer-associated mutations in speckle-type POZ protein (SPOP) regulate steroid receptor coactivator 3 protein turnover. *PNAS* **110** 6997–7002. (<https://doi.org/10.1073/pnas.1304502110>)
- Geng C, Rajapakse K, Shah SS, Shou J, Eedunuri VK, Foley C, Fiskus W, Rajendran M, Chew SA, Zimmermann M, *et al.* 2014 Androgen receptor is the key transcriptional mediator of the tumor suppressor SPOP in prostate cancer. *Cancer Research* **74** 5631–5643. (<https://doi.org/10.1158/0008-5472.CAN-14-0476>)
- Geng C, Kaochar S, Li M, Rajapakse K, Fiskus W, Dong J, Foley C, Dong B, Zhang L, Kwon OJ, *et al.* 2017 SPOP regulates prostate epithelial cell proliferation and promotes ubiquitination and turnover of c-MYC oncoprotein. *Oncogene* **36** 4767–4777. (<https://doi.org/10.1038/onc.2017.80>)
- Gu G, Yuan J, Wills M & Kasper S 2007 Prostate cancer cells with stem cell characteristics reconstitute the original human tumor in vivo. *Cancer Research* **67** 4807–4815. (<https://doi.org/10.1158/0008-5472.CAN-06-4608>)
- He B, Lanz RB, Fiskus W, Geng C, Yi P, Hartig SM, Rajapakse K, Shou J, Wei L, Shah SS, *et al.* 2014 GATA2 facilitates steroid receptor coactivator recruitment to the androgen receptor complex. *PNAS* **111** 18261–18266. (<https://doi.org/10.1073/pnas.1421415111>)
- Hepburn AC, Steele RE, Veeratterapillay R, Wilson L, Kounatidou EE, Barnard A, Berry P, Cassidy JR, Moad M, El-Sherif A, *et al.* 2019 The induction of core pluripotency master regulators in cancers defines poor clinical outcomes and treatment resistance. *Oncogene* **38** 4412–4424. (<https://doi.org/10.1038/s41388-019-0712-y>)
- Jafari R, Almqvist H, Axelsson H, Ignatshchenko M, Lundback T, Nordlund P & Martinez Molina D 2014 The cellular thermal shift assay for evaluating drug target interactions in cells. *Nature Protocols* **9** 2100–2122. (<https://doi.org/10.1038/nprot.2014.138>)
- Jeter CR, Liu B, Liu X, Chen X, Liu C, Calhoun-Davis T, Repass J, Zaehres H, Shen JJ & Tang DG 2011 NANOG promotes cancer stem cell characteristics and prostate cancer resistance to androgen deprivation. *Oncogene* **30** 3833–3845. (<https://doi.org/10.1038/onc.2011.114>)
- Jeter CR, Liu B, Lu Y, Chao HP, Zhang D, Liu X, Chen X, Li Q, Rycak K, Calhoun-Davis T, *et al.* 2016 NANOG reprograms prostate cancer cells to castration resistance via dynamically repressing and engaging the AR/FOXO1 signaling axis. *Cell Discovery* **2** 16041. (<https://doi.org/10.1038/celldisc.2016.41>)
- Jiang MY, Lee TL, Hao SS, Mahooti S, Baird SM, Donoghue DJ & Haas M 2016 Visualization of early prostatic adenocarcinoma as a stem cell disease. *Oncotarget* **7** 76159–76168. (<https://doi.org/10.18632/oncotarget.12709>)
- Ju X, Ertel A, Casimiro MC, Yu Z, Meng H, McCue PA, Walters R, Fortina P, Lisanti MP & Pestell RG 2013 Novel oncogene-induced metastatic prostate cancer cell lines define human prostate cancer progression signatures. *Cancer Research* **73** 978–989. (<https://doi.org/10.1158/0008-5472.CAN-12-2133>)
- Kaochar S, Dong J, Torres M, Rajapakse K, Nikolos F, Davis CM, Ehli EA, Coarfa C, Mitsiades N & Poulaki V 2018 ICG-001 exerts potent anticancer activity against uveal melanoma cells. *Investigative Ophthalmology and Visual Science* **59** 132–143. (<https://doi.org/10.1167/iov.17-22454>)
- Koh CM, Gurel B, Sutcliffe S, Aryee MJ, Schultz D, Iwata T, Uemura M, Zeller KI, Anele U, Zheng Q, *et al.* 2011 Alterations in nucleolar structure and gene expression programs in prostatic neoplasia are driven by the MYC oncogene. *American Journal of Pathology* **178** 1824–1834. (<https://doi.org/10.1016/j.ajpath.2010.12.040>)
- Kranzbuhler B, Salemi S, Mortezaei A, Sulser T & Eberli D 2019 Combined N-terminal androgen receptor and autophagy inhibition increases the antitumor effect in enzalutamide sensitive and enzalutamide resistant prostate cancer cells. *Prostate* **79** 206–214. (<https://doi.org/10.1002/pros.23725>)
- Kregel S, Szmulowitz RZ & Vander Griend DJ 2014 The pluripotency factor Nanog is directly upregulated by the androgen receptor in prostate cancer cells. *Prostate* **74** 1530–1543. (<https://doi.org/10.1002/pros.22870>)
- Kuser-Abali G, Alptekin A, Lewis M, Garraway IP & Cinar B 2015 YAP1 and AR interactions contribute to the switch from androgen-dependent to castration-resistant growth in prostate cancer. *Nature Communications* **6** 8126. (<https://doi.org/10.1038/ncomms9126>)
- Lin SC, Kao CY, Lee HJ, Creighton CJ, Ittmann MM, Tsai SJ, Tsai SY & Tsai MJ 2016 Dysregulation of miRNAs-COUP-TFII-FOXO1-CENPF axis contributes to the metastasis of prostate cancer. *Nature Communications* **7** 11418. (<https://doi.org/10.1038/ncomms11418>)

- Ma F, Ye H, He HH, Gerrin SJ, Chen S, Tanenbaum BA, Cai C, Sowalsky AG, He L, Wang H, *et al.* 2016 SOX9 drives WNT pathway activation in prostate cancer. *Journal of Clinical Investigation* **126** 1745–1758. (<https://doi.org/10.1172/JCI78815>)
- Mazzu YZ, Armenia J, Chakraborty G, Yoshikawa Y, Coggins SA, Nandakumar S, Gerke TA, Pomerantz MM, Qiu X, Zhao H, *et al.* 2019 A novel mechanism driving poor-prognosis prostate cancer: overexpression of the DNA repair gene, ribonucleotide reductase small subunit M2 (RRM2). *Clinical Cancer Research* **25** 4480–4492. (<https://doi.org/10.1158/1078-0432.CCR-18-4046>)
- Nguyen HG, Yang JC, Kung HJ, Shi XB, Tilki D, Lara Jr PN, DeVere White RW, Gao AC & Evans CP 2014 Targeting autophagy overcomes Enzalutamide resistance in castration-resistant prostate cancer cells and improves therapeutic response in a xenograft model. *Oncogene* **33** 4521–4530. (<https://doi.org/10.1038/onc.2014.25>)
- Nickel J, Gohlke BO, Erehman J, Banerjee P, Rong WW, Goede A, Dunkel M & Preissner R 2014 SuperPred: update on drug classification and target prediction. *Nucleic Acids Research* **42** W26–W31. (<https://doi.org/10.1093/nar/gku477>)
- Perez-Stable CM, Pozas A & Roos BA 2000 A role for GATA transcription factors in the androgen regulation of the prostate-specific antigen gene enhancer. *Molecular and Cellular Endocrinology* **167** 43–53. ([https://doi.org/10.1016/S0303-7207\(00\)00300-2](https://doi.org/10.1016/S0303-7207(00)00300-2))
- Sambhi MP, Kannan R, Thananopavarn C, Ookhtens M & Gudenzi M 1989 Therapeutic tolerance, hemodynamic effects, and oral dose kinetics of dilazep dihydrochloride in hypertensive patients. *Journal of Pharmaceutical Sciences* **78** 281–284. (<https://doi.org/10.1002/jps.2600780404>)
- Sanchez BG, Bort A, Vara-Ciruelos D & Diaz-Laviada I 2020 Androgen deprivation induces reprogramming of prostate cancer cells to stem-like cells. *Cells* **9** 1441. (<https://doi.org/10.3390/cells9061441>)
- Siegel RL, Miller KD, Fuchs HE & Jemal A 2021 Cancer statistics, 2021. *CA: A Cancer Journal for Clinicians* **71** 7–33. (<https://doi.org/10.3322/caac.21654>)
- Soler M, Mancini F, Meca-Cortes O, Sanchez-Cid L, Rubio N, Lopez-Fernandez S, Lozano JJ, Blanco J, Fernandez PL & Thomson TM 2009 HER3 is required for the maintenance of neuregulin-dependent and -independent attributes of malignant progression in prostate cancer cells. *International Journal of Cancer* **125** 2565–2575. (<https://doi.org/10.1002/ijc.24651>)
- Sotomayor P, Godoy A, Smith GJ & Huss WJ 2009 Oct4A is expressed by a subpopulation of prostate neuroendocrine cells. *Prostate* **69** 401–410. (<https://doi.org/10.1002/pros.20895>)
- Subramanian A, Tamayo P, Mootha VK, Mukherjee S, Ebert BL, Gillette MA, Paulovich A, Pomeroy SL, Golub TR, Lander ES, *et al.* 2005 Gene set enrichment analysis: a knowledge-based approach for interpreting genome-wide expression profiles. *PNAS* **102** 15545–15550. (<https://doi.org/10.1073/pnas.0506580102>)
- Taylor BS, Schultz N, Hieronymus H, Gopalan A, Xiao Y, Carver BS, Arora VK, Kaushik P, Cerami E, Reva B, *et al.* 2010 Integrative genomic profiling of human prostate cancer. *Cancer Cell* **18** 11–22. (<https://doi.org/10.1016/j.ccr.2010.05.026>)
- Tsai FY & Orkin SH 1997 Transcription factor GATA-2 is required for proliferation/survival of early hematopoietic cells and mast cell formation, but not for erythroid and myeloid terminal differentiation. *Blood* **89** 3636–3643.
- Tsai FY, Keller G, Kuo FC, Weiss M, Chen J, Rosenblatt M, Alt FW & Orkin SH 1994 An early haematopoietic defect in mice lacking the transcription factor GATA-2. *Nature* **371** 221–226. (<https://doi.org/10.1038/371221a0>)
- Umetani M, Nakao H, Doi T, Iwasaki A, Ohtaka M, Nagoya T, Mataka C, Hamakubo T & Kodama T 2000 A novel cell adhesion inhibitor, K-1714, reduces the endothelial VCAM-1 induction by inflammatory cytokines, acting through the regulation of GATA. *Biochemical and Biophysical Research Communications* **272** 370–374. (<https://doi.org/10.1006/bbrc.2000.2784>)
- Varambally S, Dhanasekaran SM, Zhou M, Barrette TR, Kumar-Sinha C, Sanda MG, Ghosh D, Pienta KJ, Sewalt RG, Otte AP, *et al.* 2002 The polycomb group protein EZH2 is involved in progression of prostate cancer. *Nature* **419** 624–629. (<https://doi.org/10.1038/nature01075>)
- Vidal SJ, Rodriguez-Bravo V, Quinn SA, Rodriguez-Barrueco R, Lujambio A, Williams E, Sun X, de la Iglesia-Vicente J, Lee A, Readhead B, *et al.* 2015 A targetable GATA2-IGF2 axis confers aggressiveness in lethal prostate cancer. *Cancer Cell* **27** 223–239. (<https://doi.org/10.1016/j.ccell.2014.11.013>)
- Wang Q, Li W, Liu XS, Carroll JS, Janne OA, Keeton EK, Chinnaiyan AM, Pienta KJ & Brown M 2007 A hierarchical network of transcription factors governs androgen receptor-dependent prostate cancer growth. *Molecular Cell* **27** 380–392. (<https://doi.org/10.1016/j.molcel.2007.05.041>)
- Wang H, Leav I, Ibaragi S, Wegner M, Hu GF, Lu ML, Balk SP & Yuan X 2008 SOX9 is expressed in human fetal prostate epithelium and enhances prostate cancer invasion. *Cancer Research* **68** 1625–1630. (<https://doi.org/10.1158/0008-5472.CAN-07-5915>)
- Wang Q, Li W, Zhang Y, Yuan X, Xu K, Yu J, Chen Z, Beroukhim R, Wang H, Lupien M, *et al.* 2009 Androgen receptor regulates a distinct transcription program in androgen-independent prostate cancer. *Cell* **138** 245–256. (<https://doi.org/10.1016/j.cell.2009.04.056>)
- Wang H, Zhang C, Rorick A, Wu D, Chiu M, Thomas-Ahner J, Chen Z, Chen H, Clinton SK, Chan KK, *et al.* 2011 CCI-779 inhibits cell-cycle G2-M progression and invasion of castration-resistant prostate cancer via attenuation of UBE2C transcription and mRNA stability. *Cancer Research* **71** 4866–4876. (<https://doi.org/10.1158/0008-5472.CAN-10-4576>)
- Wu D, Sunkel B, Chen Z, Liu X, Ye Z, Li Q, Grenade C, Ke J, Zhang C, Chen H, *et al.* 2014 Three-tiered role of the pioneer factor GATA2 in promoting androgen-dependent gene expression in prostate cancer. *Nucleic Acids Research* **42** 3607–3622. (<https://doi.org/10.1093/nar/gkt1382>)
- Xiao L, Feng Q, Zhang Z, Wang F, Lydon JP, Ittmann MM, Xin L, Mitsiades N & He B 2016 The essential role of GATA transcription factors in adult murine prostate. *Oncotarget* **7** 47891–47903. (<https://doi.org/10.18632/oncotarget.10294>)
- Xu K, Wu ZJ, Groner AC, He HH, Cai C, Lis RT, Wu X, Stack EC, Loda M, Liu T, *et al.* 2012 EZH2 oncogenic activity in castration-resistant prostate cancer cells is Polycomb-independent. *Science* **338** 1465–1469. (<https://doi.org/10.1126/science.1227604>)
- Yu J, Yu J, Mani RS, Cao Q, Brenner CJ, Cao X, Wang X, Wu L, Li J, Hu M, *et al.* 2010 An integrated network of androgen receptor, polycomb, and TMPRSS2-ERG gene fusions in prostate cancer progression. *Cancer Cell* **17** 443–454. (<https://doi.org/10.1016/j.ccr.2010.03.018>)
- Zadvornyi TV, Lukianova NY, Borikun TV, Vitruk YV, Stakhovskiy EO & Chekhun VF 2020 NANOG as prognostic factor of prostate cancer course. *Experimental Oncology* **42** 94–100. (<https://doi.org/10.32471/exp-oncology.2312-8852.vol-42-no-2.14673>)
- Zhao JC, Fong KW, Jin HJ, Yang YA, Kim J & Yu J 2016 FOXA1 acts upstream of GATA2 and AR in hormonal regulation of gene expression. *Oncogene* **35** 4335–4344. (<https://doi.org/10.1038/onc.2015.496>)
- Zhou HJ, Yan J, Luo W, Ayala G, Lin SH, Erdem H, Ittmann M, Tsai SY & Tsai MJ 2005 SRC-3 is required for prostate cancer cell proliferation and survival. *Cancer Research* **65** 7976–7983. (<https://doi.org/10.1158/0008-5472.CAN-04-4076>)

Received in final form 12 September 2021

Accepted 12 October 2021

Accepted Manuscript published online 12 October 2021